Density relaxation in a vibrated granular material

James B. Knight, Christopher G. Fandrich, Chun Ning Lau, Heinrich M. Jaeger, and Sidney R. Nagel
The James Franck Institute and the Department of Physics, The University of Chicago, Chicago, Illinois 60637
(Received 1 September 1994)

We report measurements of the density of a vibrated granular material as a function of time. The material studied consists of monodisperse spherical glass particles confined to a long, thin cylindrical tube. Vibrations cause the pile to evolve from a low density initial configuration toward a steady state with a final density that depends on the intensity of the vibrations. We find a complex time evolution that is incompatible with a single exponential relaxation. There appears to be a characteristic value of the acceleration that separates two regimes of packing behavior. The results are compared to current theories of compaction.

The manner in which a disordered system progresses from an initial perturbed configuration toward its equilibrium state can often be a slow and complicated process with a number of different relaxation mechanisms proceeding in parallel. Practically all work studying such relaxation phenomena has focused on thermal systems in which the concepts of temperature and equilibrium are well defined. Comparatively little is known about relaxation in nonthermal disordered systems. A simple prototype of such systems is a box filled with a granular material such as sand or ball bearings where the material inside the box can be assembled in many ways [1]. Indeed, for the case of spherical particles, one can vary the packing fraction from $\rho \approx 0.55$ for the mechanically least stable configurations to $\rho \approx 0.64$ for the densest, random close packing limit [2]. The gravitational energy necessary to lift a single grain of sand by one diameter exceeds any thermal energy available at room temperature by at least 12 orders of magnitude, so that temperature-induced fluctuations offer no means of moving between the many metastable states available to the particles. As a result, the granular system can evolve along a sequence of metastable configurations only in the presence of externally applied, nonthermal excitations produced, for example, by shaking or vibrating the container. We address the question of how such a system approaches its optimally packed state for a given vibration intensity.

Despite the fundamental importance of compaction and settling to many industrial processes using granular materials, experimental work to characterize this evolution in vibrated granular media is sparse and inconclusive [3,4]. On the theoretical side there have been efforts [5] to use concepts from statistical mechanics in the description of granular media, but only recently has there been an attempt, by Edwards and co-workers, to formulate a "thermodynamics of powders" [6]. In order to realize such a theory, it is necessary to know the phenomenology of how powders compact under a variety of experimental conditions.

In this paper, we present a systematic experimental investigation of the evolution of density with time in a vibrated granular material. We use a noninvasive, capacitive technique to measure the density of a simple model system in which the constituent particles are monodisperse spheres. We focus on the relaxation occurring when the system is prepared in a low density state and then vibrated to induce decay toward the steady state density [7]. The data indicate a characteristic, nonexponential relaxation process that depends on both the strength of the vibration, parametrized by the acceleration, and the depth from the surface into the pile. We expect that the understanding obtained from this simple model system may be generically applicable to more complicated granular materials.

Monodisperse, 2 mm diameter spherical soda-lime glass beads were confined to a 1.88 cm diameter Pyrex tube mounted vertically on a Brüel and Kjaer 4808 vibration exciter. A schematic diagram of the apparatus is shown in Fig. 1(a). Since water vapor in the tube can introduce cohesion between the beads and change their frictional properties as well as the dielectric response of the bead pack, the beads were baked prior to loading in the tube and maintained under vacuum to isolate the system from external humidity fluctuations. The tube was 1 m in length and constrained to vertical motion by two Teflon linear motion guides. In order to minimize electrostatic attraction between the beads and the tube walls, the inner surface of the tube was periodically treated with an antistatic solution. The beads were prepared in a low density initial state by flowing high pressure, dry nitrogen gas through the tube from the bottom. The initial height of the beads before tapping was 87 cm, corresponding to an initial column packing fraction of 0.577 ± 0.005. This is not the loosest packing that could be achieved, but proved to be an easily reproducible value so that repeated measurements starting from the same initial conditions could be made. The smooth tube walls and the low static friction combined to prevent convection [8]. We verified that no convection occurred by using dyed tracer beads to visualize any large scale flow.

The vibration and measurement portions of the apparatus were computer controlled to facilitate runs of long duration. The output signal from a computer-triggered function generator, consisting of one complete

cycle of a 30 Hz sine wave, was amplified and fed to the electromagnetic vibration exciter, producing a single shake, or "tap." The intensity of these taps was monitored with an accelerometer. The acceleration profile of a representative tap is shown in the inset of Fig. 1(a). We parametrized the vibration intensity by Γ, the ratio of a, the peak acceleration of a tap [9], to $g = 9.81$ m/s^2, the gravitational acceleration ($\Gamma \equiv a/g$). The use of individual, well separated taps avoided problems with internal resonances that are likely to occur during continuous driving of a long tube. Furthermore, using discrete taps

allowed sufficient time between excitations so that all motion in the column from one tap ceased before the next tap started; the measurements described here were therefore not affected by any motion caused by one tap intruding into the interval of the next tap.

The column density was measured with four parallel plate capacitors composed of copper tape strips mounted along the outside of the tube. Since the capacitance of a capacitor depends on the dielectric constant of the material between its plates, this device is ideal for measuring the density of the material inside the tube in a nonin-
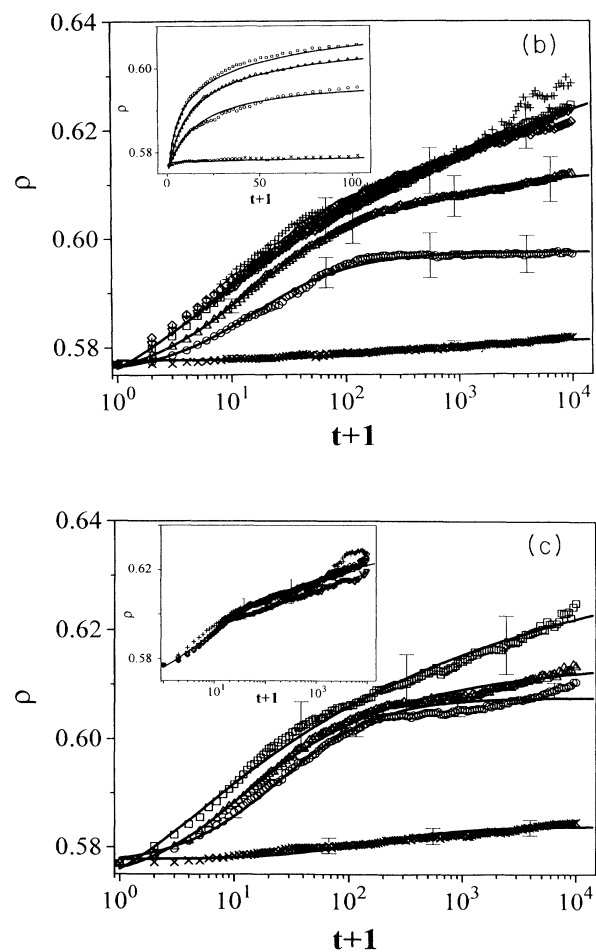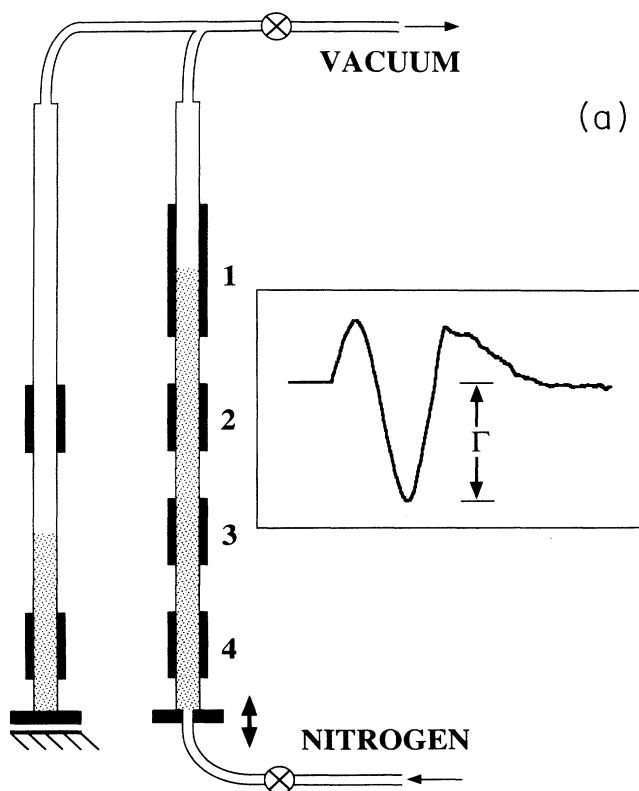

FIG. 1. (a) A schematic drawing of the apparatus showing the cylindrical container and the four measuring capacitors. Two reference capacitors are used to correct for long term drifts of the system. The inset shows the acceleration induced by a tap of $\Gamma = 2.7$. This profile was obtained with an accelerometer mounted on the stage of the vibration exciter and is an average of 64 pulses. (b) The packing fraction ρ from capacitor 4 (near the bottom of the tube) as a function of the logarithm of the tap number t for $\Gamma = 1.4$ ($\times$), 1.8 ($\bigcirc$), 2.3 ($\triangle$), 2.7 ($\square$), 3.1 (∇), 4.5 ($\Diamond$), and 5.4 ($+$). The tap number is offset by one tap so that the origin is included in the figure. This convention is followed in all the figures. Each curve is an average of 4 to 5 separate experimental runs and the error bars represent the rms variations between runs. We emphasize that this variation is illustrative of the range of packing profiles exhibited at any Γ, and not of fluctuations within individual runs. The solid lines are least square fits to the heuristic form, Eq. (3), explained in the text. The inset shows a subset of the data on a linear scale. (c) The packing fraction obtained from capacitor 2 near the top of the tube. The data for $\Gamma = 1.4$ ($\times$), 1.8 ($\bigcirc$), 2.3 ($\triangle$), and 2.7 ($\square$) are shown in the main figure and the data for $\Gamma = 2.7$ ($\square$), 3.1 (∇), 4.5 ($\Diamond$), and 5.4 ($+$) are shown in the inset. As in Fig. 1(b), the solid lines are fits to Eq. (3).

vasive manner. Capacitor 1 had plates 30 cm in length and 1.2 cm in width, and its center was positioned 80 cm above the bottom of the tube such that the top surface of the bead pack remained between the two plates throughout the compaction process. It was calibrated with optical measurements of the total column height during every run, and was employed only to track the column height. The plates of capacitors 2, 3, and 4, mounted below capacitor 1 with their centers 50, 30, and 10 cm from the bottom of the tube, were each 15 cm long and 1.2 cm wide. Each of these capacitors covered about 17% of the system, and averaged the density over sections containing approximately 6000 beads. In separate measurements, we verified that the capacitance varied linearly with packing fraction for each capacitor.

An *LCR* meter was used to measure the capacitances of all the capacitors between taps. The capacitances of two reference capacitors were also measured simultaneously to correct for temperature fluctuations and short term (within a single run) drift in the measurement electronics. These capacitors were mounted on a stationary Pyrex tube identical to the vibrated one [see Fig. 1(a)]. One of the reference capacitors was filled with 2 mm glass beads while the other remained empty. Both tubes were maintained under the same vacuum. With these arrangements, the resolution of our measurement was 1 fF, and the conversion factor between capacitance and packing fraction for capacitors 2, 3, and 4 was measured to be $(6.0\pm0.3)\times10^{-4}$ fF^{-1}. We used the average column density, obtained directly by optical measurements of the initial total column height, as the initial density ρ_0 for each of the buried capacitors. Fluctuations in the absolute values for the initial packing fractions were on the order of 0.005 from run to run.

Figure 1(b) shows the packing fraction ρ near the bottom of the tube (capacitor 4) as a function of tap number t for Γ between 1.4 and 5.4. Each curve is an average of 5 separate runs and the error bars (shown only for a few points) represent the rms variations between individual runs. These variations do not, however, reflect fluctuations within individual curves of the ensemble, which are typically smooth within the resolution of the capacitors and have the same characteristic shape as the average curve shown in the figure. The tap number is plotted on a logarithmic scale so that four decades of t can be easily viewed. The tap number t is offset by 1 tap so that the origin is included on the logarithmic axis. This convention is followed throughout the paper. For comparison, the inset shows a subset of the data on a linear scale. Plotted in this way over the full range of t, however, most of the complex behavior apparent in Fig. 1(b) is obscured. At the lowest acceleration in Fig. 1(b), $\Gamma=1.4$, significant relaxation was clearly observed, but only after tapping for a long time. At $\Gamma=1.8$, the behavior changed radically; the density began to increase immediately and continued until $t=200$, at which time the density variation slowed down dramatically. (We note that in individual runs out to $t=100\,000$, slow density changes similar to that for $\Gamma=1.4$ can continue at all accelerations.) The $\Gamma=2.3$ data show no sign of saturation even out to $t=10\,000$. At $\Gamma=2.7$ and above, all the

curves appear to lie on a common curve. At the highest acceleration, $\Gamma=5.4$, fluctuations about this average curve begin to be seen. At time scales longer than recorded for these measurements, it is conceivable that these curves no longer continue to superimpose on top of one another.

The density relaxation near the top of the tube, measured with capacitor 2, is shown in Fig. 1(c). The sharp transition in packing behavior between $\Gamma=1.4$ and $\Gamma=1.8$ observed at the bottom of the tube [Fig. 1(b)] persists, but the differences between the $\Gamma=1.8$ and $\Gamma=2.3$ data are now smaller. Again, the higher acceleration runs collapse to a single curve within the statistical spread, but the curves for $\Gamma\geq3.1$ are noisier than those of capacitor 4 near the bottom of the tube. This reflects the onset of significant fluctuations in the individual runs contributing to the ensemble average. It is evident from Fig. 1 that no steady state has been attained at the
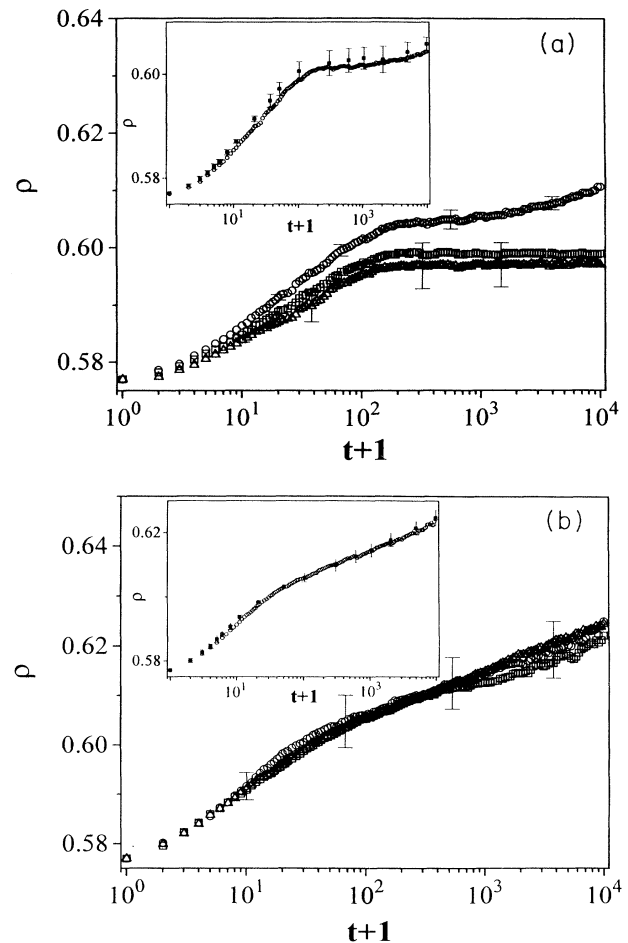

FIG. 2. (a) The dependence of the packing fraction for $\Gamma=1.8$ obtained from the capacitor 2 ($\bigcirc$), capacitor 3 ($\times$), and capacitor 4 ($\triangle$). The inset shows the column density for $\Gamma=1.8$ determined from a weighted averaged of the data from the three lowest capacitors ($\bigcirc$) compared with an independent measurement of the average density determined by the height of the grains in the column ($\square$). (b) The same data as Fig. 2(a) for $\Gamma=2.7$.

higher accelerations up to $t = 10\,000$.

The depth dependence of the packing fraction is shown in more detail for $\Gamma = 1.8$ in Fig. 2(a). Clearly, the net density change decreases as the depth increases. The separation between the packing curves for capacitors at increasing depth is very similar to that seen in Fig. 1(b) for decreasing acceleration. At higher accelerations the column packs more homogeneously [shown in Fig. 2(b) for $\Gamma = 2.7$] and at the same rate for all the capacitors within the statistical uncertainty. Previous measurements of depth dependence in granular compaction employed invasive measurement techniques, which limited data resolution, and failed to control for convection and size segregation. Nevertheless, there is some general agreement between their results and ours in that the density change is higher near the top of the system [4,10].

As a check on the reliability of absolute density values obtained from our measurements, we have calculated the average column density using the calibrated measurements of capacitors 2, 3, and 4. (The density observed in capacitor 2 was extrapolated to the top of the column.) The inset of Fig. 2(a) shows a comparison for $\Gamma = 1.8$ of this average column density with independent measurements of the column density obtained from optical measurements of the column height. The agreement is well within error. The inset of Fig. 2(b) contains the same comparison for $\Gamma = 2.7$.

The nature of the transition in packing behavior around $\Gamma = 1.8$ is clarified by plotting the change in packing fraction after 10 000 taps, $\Delta\rho(t = 10\,000)$ $= \rho(t = 10\,000) - \rho_0$, against acceleration Γ. This is shown in Fig. 3 for both the overall column density and the density at the bottom of the tube measured by capacitor 4. A rapid increase in the average column density occurs at a characteristic acceleration $\Gamma_c \approx 1.8$. The value of this characteristic acceleration near the bottom of the tube, measured by capacitor 4, is slightly higher. (Much of the previous experimental work in granular compaction concentrated on establishing profiles of this
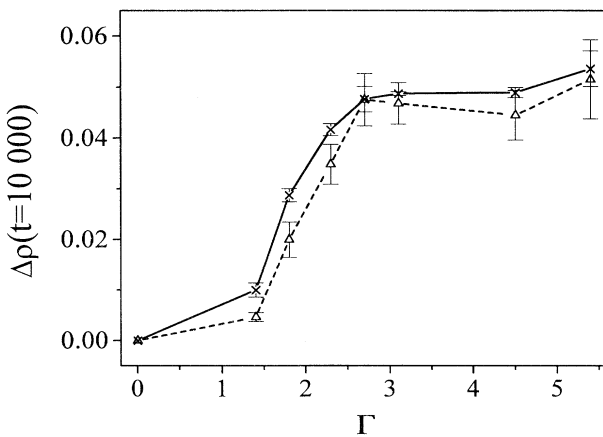
type [4,10–12], albeit under less controlled experimental conditions and with far less data density. Reported values for Γ_c generally lie between $\Gamma = 1.0, 2.0$. We have found that the precise value of Γ_c is sensitive to changes in the frictional interaction between the beads and between the beads and the container wall.) Above $\Gamma \approx 2.7$, $\Delta\rho(t = 10\,000)$ levels off in both curves shown in Fig. 3. However, our experiment probed only the regime of low shaking intensity where gravity and internal friction are significant forces and convective motion can be controlled. At higher accelerations, $\Gamma \gg \Gamma_c$, defect creation competes with defect "annealing" during each tap, and we expect $\Delta\rho(t = 10\,000)$ to decrease upon further acceleration increase [4,12,13].

Although there have been many simulations of granular convection and size segregation [14,15], there have been only a few attempts at simulating granular compaction. Barker and Mehta [15–17] have employed a nonsequential, random close packing algorithm that permits the formation of arches and other complex structures to model the relaxation of a tapped, three dimensional pack composed of frictionless, monodisperse spheres. Their results were obtained for the regime $\Gamma \gg \Gamma_c$, and exhibit a steady decrease in $\Delta\rho$ with increasing tap intensity. This is the opposite trend to what we have observed, which we attribute to the simulations being performed at much larger accelerations than our experiments. Nevertheless, for any chosen shaking intensity, these simulations produce time evolutions $\rho(t)$ that exhibit slow relaxation behavior and are qualitatively very similar to our data.

The traces in Fig. 1(b) clearly indicate that a simple exponential relaxation arising from a single characteristic decay time does not describe granular compaction. There are many possibilities for metastable bead configurations to evolve under tapping, suggesting that several, and possibly a whole range of, time constants may be more appropriate. Barker and Mehta have recently proposed [17] a model in which beads can relax both independently, as individual particles, and collectively, as clusters. Their model, with time scales τ_{ind} for single-bead relaxation and τ_{col} for cluster relaxation, leads to a sum of two exponential terms, so that

$$\rho(t) = \rho_f - \Delta\rho_{\mathrm{ind}}\exp\left[-\frac{t}{\tau_{\mathrm{ind}}}\right] - \Delta\rho_{\mathrm{col}}\exp\left[-\frac{t}{\tau_{\mathrm{col}}}\right], \quad (1)$$

where ρ_f is the final steady state density and $\Delta\rho_{\mathrm{ind}}$ and $\Delta\rho_{\mathrm{col}}$ are the amplitudes of the two relaxation processes. Figure 4(a) shows the best fits of $\rho(t)$ from Eq. (1) to several relaxation curves representative of the range of our observed packing behavior. Although the resulting fits lie well within experimental spread from run to run, they exhibit additional structure not contained in the ensemble averages. Furthermore, the large number of fitting parameters (5) and the systematic deviations in curvature apparent for $\Gamma \geq 2.3$ render the agreement inconclusive.

Stretched exponential fits have been commonly applied to relaxation processes in disordered thermal systems [18] and are characteristic of a continuous range of time con-

FIG. 3. $\Delta\rho(t = 10\,000)$, the change in packing fraction after 10 000 taps, is plotted against acceleration Γ. Both the overall column density ($\times$), determined by the height of the grains in the column, and the density determined from capacitor 4 ($\triangle$) are shown.

stants. We find that the form

$$\rho(t)=\rho_f-\Delta\rho_\infty\exp\left[-\left[\frac{t+t_0}{\tau}\right]^\beta\right] \qquad (2)$$

fits our data reasonably well where we have allowed the zero of our tap number counting to be adjustable by t_0 taps, with t_0 assumed positive [see Fig. 4(b)]. However, as in the case of the double exponential fits shown in Fig. 4(a), systematic deviations from the ensemble-averaged data remain, and the equally large number of fitting parameters renders the agreement inconclusive as well.

An alternate model for granular relaxation by Hong et al. [19] is based on a diffusing void picture. It predicts a power law dependence of the column height reduction, Δh, with time: $\Delta h \propto t^z$, where the exponent $z = 1$ was obtained from numerical simulations. Because in our experiments Δh is small relative to the overall column height, we find that plots of $\Delta h(t)$ have the same general shape as those corresponding to $1/\Delta\rho(t)$, where $\Delta\rho(t) =\rho(t)-\rho_0$ is the change in packing fraction. The inset of Fig. 1(b) can therefore serve as an illustration of our measurements of $\Delta h(t)$: we observe a rapid initial change in height followed by increasingly slower packing. A single power law is not a good fit to our data.
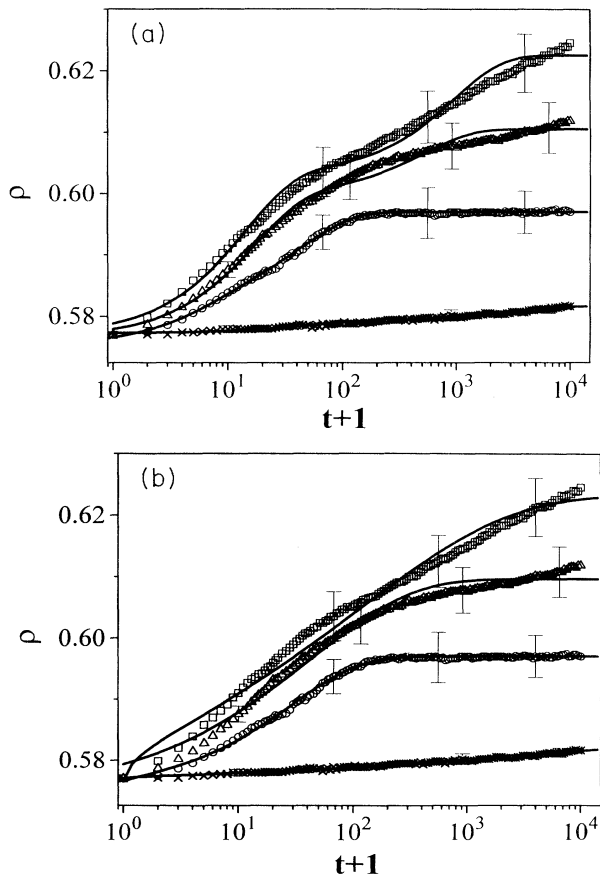

FIG. 5. The parameters B ($\circ$) and τ ($\times$), obtained from a fit of Eq. (3) to the density measured by capacitor 2 [see Fig. 1(c)], are plotted vs Γ. The inset shows the parameters ρ_f ($\square$) and $\Delta\rho_\infty$ (+) from the same fits, also plotted against Γ. At the higher values of Γ, ρ_f is larger than the random close packing limit (≈ 0.64). This is not unphysical, however, as ordered close packing can occur along the container walls.

Finally, we note that a very reasonable four-parameter fit to the whole range of data is obtained with the heuristic expression

$$\rho(t)=\rho_f-\frac{\Delta\rho_\infty}{1+B\ln\left[1+\dfrac{t}{\tau}\right]} , \qquad (3)$$

where the parameters ρ_f, $\Delta\rho_\infty$, B, and τ are constants that depend only on the acceleration Γ. This form is motivated by the observation of large time intervals of logarithmically slow relaxation in Figs. 1 and 2, followed by a crossover to a steady state at the longest times. The solid lines through the data in Figs. 1(b) and 1(c) are fits to Eq. (3). Figure 5 and its inset show the Γ dependence

FIG. 4. Least squares fits of our data for several representative values of acceleration, Γ, to (a) Eq. (1) by Barker and Mehta [17] and (b) to the stretched exponential form, Eq. (2), explained in the text.
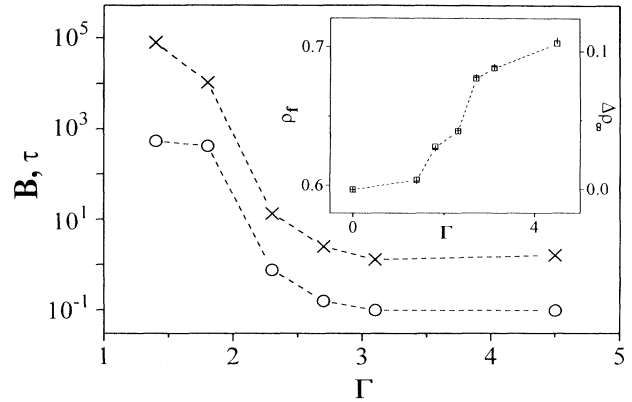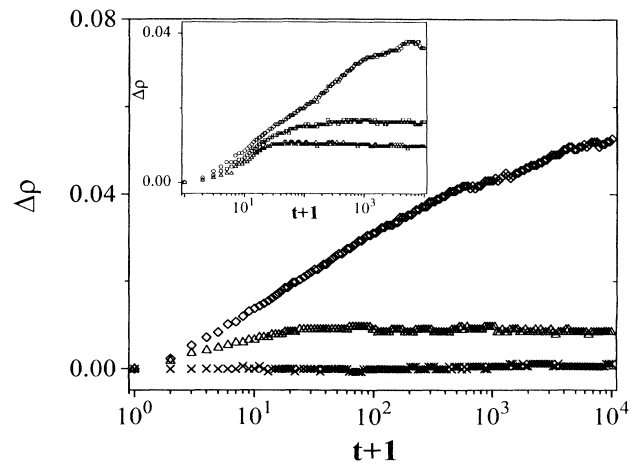

FIG. 6. The increase in packing fraction $\Delta\rho$ from capacitor 4 (near the bottom of the tube) for 0.5 mm glass beads as a function of the logarithm of the tap number t (offset by 1), for $\Gamma=1.4$ ($\times$), 2.3 ($\triangle$), and 3.5 ($\Diamond$). Each curve represents a single run. The inset shows $\Delta\rho$ for the same beads obtained from capacitor 2 ($\circ$), capacitor 3 ($\square$), and capacitor 4 ($\triangle$) at $\Gamma=1.8$.

of B, τ, ρ_f, and $\Delta\rho_\infty$ for the fits of Eq. (3) to the capacitor 2 density data. Qualitatively similar curves are found for the data from capacitor 4. In all cases, these parameters vary monotonically with Γ, and the fits are generally better than those obtained with either Eq. (1) or (2), which each have an additional adjustable parameter. Logarithmic relaxation has also previously been observed in the decay of the slope of a vibrated sandpile [20].

The focus on this paper has been on the density relaxation of 2 mm glass spheres in a 1.88 cm diameter Pyrex tube, but we have performed relaxation experiments with varying sizes of glass beads and aluminum oxide particles (with a rough, irregular shape) in tubes of different diameters. We find the same qualitative behavior in all these systems. As an example, we show in Fig. 6 the change in packing fraction $\Delta\rho(t)$ as a function of tap number t for 0.5 mm glass beads near the bottom (capacitor 4) of the same 1.88 cm diam Pyrex tube used for the 2 mm beads. [We have potted $\Delta\rho(t)$ because these curves are individual runs and not averages as in Figs. 1 and 2, and thus there is some indeterminacy in the absolute value of the initial packing fraction.] The same general curve shapes are observed for the smaller particles as were seen in Fig. 1(b) for the larger ones, indicating that the finite size of the system is not dominating our results. The inset of Fig. 6 is a plot of $\Delta\rho$ as a function of tap number t for capacitors 2, 3, and 4 at $\Gamma = 1.8$. The inhomogeneous packing is analogous to that observed in Fig. 2(a) for the 2 mm beads.

In conclusion, we have observed that density relaxation in even the simplest of granular materials, a monodisperse bead pack, is highly complex. The change in packing fraction $\Delta\rho(t = 10\,000)$ increases sharply and levels off as the shaking intensity, parametrized by the peak acceleration of the vibration, is increased through a characteristic value $\Gamma_c \approx 1.8$ (Fig. 3). The density of a vibrated bead pack does not decay as a single exponential curve to a steady state value [Figs. 1(b) and 1(c)]; instead, two or more time scales may be involved. The functional form that we found which gives the most satisfactory fit to our data was not theoretically motivated. We also found that the packing is not homogeneous at low accelerations. Instead, the packing fraction decreases as depth increases [Figs. 2(a) and 2(b)]. We interpret this as a gradient in the effective shaking intensity. Above Γ_c, packing appears to be homogeneous. It is interesting to speculate how the shaking intensity can be related to an effective temperature and to investigate whether the different final steady states that can be observed in such shaking experiments as ours can be related to the concept of compactivity [6,21]. This would provide an analogy with the normal thermodynamics used for systems that have a well defined temperature that determines their static properties. Some of these questions will be addressed in a later publication dealing with the fluctuations of the density around its steady value [7].

ACKNOWLEDGMENTS

[1] H. M. Jaeger and S. R. Nagel, Science **255**, 1523 (1992).

[2] G. Y. Onoda and E. G. Liniger, Phys. Rev. Lett. **64**, 2727 (1990).

[3] B. S. Neumann, in *Flow Properties of Disperse Systems*, edited by J. J. Hermans (North-Holland, Amsterdam, 1953), pp. 382–422; P. E. Evans and R. S. Millman, in *Vibratory Compacting, Volume 2*, edited by H. H. Hausner, Kempton H. Roll, and Peter K. Johnson (Plenum, New York, 1967), pp. 237–251; I. G. Shatalova, N. S. Gorbunov, and V. I. Likhtman, *ibid.*, pp. 144–149; M. Yamashiro, Y. Yuasa, and K. Kawakita, Powder Tech. **34**, 225 (1983); J. Malave, G. V. Barbosa-Canovas, and M. Peleg, J. Food Sci. **50**, 1473 (1985).

[4] R. Dobry and R. V. Whitman, Department of Civil Engineering, M.I.T. Research Report R70-05, Soils Publication 251, 1969 (unpublished); E. W. Brand, in *Evaluation of Relative Density and Its Role in Geotechnical Projects Involving Cohesionless Soils*, edited by E. T. Selig and R. S. Ladd, ASTM Special Technical Publication No. 523 (American Society for Testing and Materials, Baltimore, 1973), pp. 121–131.

[5] Ken-Ichi Kanatani, Powder Tech. **30**, 217 (1981); M. Shahinpoor, *ibid.* **25**, 163 (1980).

[6] S. F. Edwards, in *Granular Matter, An Interdisciplinary Approach*, edited by Anita Mehta (Springer-Verlag, New York, 1994), pp. 121–140.

[7] In this case, the total change in density is far greater than the steady-state density fluctuations that occur in the driven system. That is, we are observing irreversible relaxation toward a steady state, as opposed to small fluctuations about a steady state. We will present work on the linear response regime in a later paper. J. B. Knight, E. Nowak, E. Ben-Naim, H. M. Jaeger, and S. R. Nagel (unpublished).

[8] J. B. Knight, H. M. Jaeger, and S. R. Nagel, Phys. Rev. Lett. **70**, 3728 (1993).

[9] The parameter Γ can also be calculated using the rms acceleration of the tap; we have experimentally determined that $\Gamma_{\mathrm{rms}} = (0.293 \pm 0.002)\Gamma$. Similarly, Γ_1, the acceleration parameter calculated using the height of the first peak, can be determined from the ratio of the height of the first peak to that of the second, which we have measured to be 0.52 ± 0.02.

[10] Toshihide Tokue, Soils Found. **16**, 1 (1976); Tokue noticed that applying a load to the top of a column of vibrated granular material increased Γ_c. Similarly, the characteristic acceleration near the bottom of our tube is measurably higher than that of the total column density (Fig. 3). Al-

though a pressure head does not develop in static granular materials confined to a columnar geometry, it is possible that the sand weight is significant during vibration, and the resulting "dynamic" pressure head is responsible for the packing inhomogeneity observed in Fig. 2(a). It is not clear, however, why this pressure head is not observed for $\Gamma > 1.7$.

[11] A. Suzuki, H. Takahashi, and T. Tanaka, Powder Tech. 2, 72 (1968/69); R. Dobry and R. V. Whitman, in *Evaluation of Relative Density and Its Role in Geotechnical Projects Involving Cohesionless Soils* (Ref. [4]), pp. 156–170.

[12] D. J. D'Appolonia and E. D'Appolonia, in *Proceedings, Third Asian Regional Conference on Soil Mechanics and Foundation Engineering* (Jerusalem Academic, Jerusalem, 1967), pp. 266–268.

[13] This competition is easily seen in the two-dimensional case: H. M. Jaeger, J. B. Knight, C.-H. Liu, and S. R. Nagel, Mat. Res. Bull. 19, 25 (1994); J. Duran, T. Mazozi, E. Clement, and J. Rajchenbach, Phys. Rev. E 50, 3092 (1994).

[14] Hans J. Herrmann, in *Disorder and Granular Media*, edited by D. Bideau and A. Hansen (North-Holland, Amsterdam, 1993), pp. 305–320.

[15] G. C. Barker, in *Granular Matter, An Interdisciplinary Approach* (Ref. [6]), pp. 35–83.

[16] G. C. Barker and Anita Mehta, Phys. Rev. A 45, 3435 (1992).

[17] G. C. Barker and Anita Mehta, Phys. Rev. E 47, 184 (1993).

[18] M. H. Cohen and G. S. Grest, Phys. Rev. B 24, 4091 (1981); R. G. Palmer, D. Stein, E. Abrahams, and P. W. Anderson, Phys. Rev. Lett. 53, 958 (1984); J. T. Bendler and M. F. Shlesinger, J. Mol. Liq. 36, 37 (1987); J. Kakalios, R. A. Street, and W. B. Jackson, Phys. Rev. Lett. 59, 1037 (1987); I. A. Campbell, J.-M. Flesselles, R. Jullien, and R. Botet, Phys. Rev. B 37, 3825 (1988); V. Degiorgio, T. Bellini, R. Piazza, F. Mantegazza, and R. E. Goldstein, Phys. Rev. Lett. 64, 1043 (1990).

[19] D. C. Hong, S. Yue, J. K. Rudra, M. Y. Choi, and Y. W. Kim, Phys. Rev. E 50, 4123 (1994).

[20] H. M. Jaeger, C.-H. Liu, and S. R. Nagel, Phys. Rev. Lett. 62, 40 (1989); T. A. J. Duke, G. C. Barker, and A. Mehta, Europhys. Lett. 13, 19 (1990).

[21] A. Mehta and S. F. Edwards, Physica A 157, 1091 (1989); A. Mehta and S. F. Edwards, in *Disorder in Condensed Matter Physics*, edited by J. Blackman and J. Tagüeña (Oxford University Press, New York, 1990), pp. 155–162; A. Mehta, in *Granular Matter, An Interdisciplinary Approach* (Ref. [6]), pp. 1–33.